10-1-2020

Novel compounds in fruits of coriander (Coşkuner & Karababa) with anti-inflammatory activity

Renyikun Yuan
Guangxi Traditional Chinese Medical University

Zhenjie Liu
Guangxi Traditional Chinese Medical University

Jianping Zhao
University of Mississippi, Research Institute Pharmaceutical Science

Qin Qin Wang
Guangxi Traditional Chinese Medical University

Aiyuan Zuo
Guangxi Traditional Chinese Medical University

See next page for additional authors

Recommended Citation

Yuan, R., Liu, Z., Zhao, J., Wang, Q.-Q., Zuo, A., Huang, L., Gao, H., Xu, Q., Khan, I. A., & Yang, S. (2020). Novel compounds in fruits of coriander (Coşkuner & Karababa) with anti-inflammatory activity. Journal of Functional Foods, 73, 104145. https://doi.org/10.1016/j.jff.2020.104145

Journal of Functional Foods 73 (2020) 104145

Contents lists available at ScienceDirect

Journal of Functional Foods

journal homepage: www.elsevier.com/locate/jff

Novel compounds in fruits of coriander (Coşkuner & Karababa) with anti-inflammatory activity

Renyikun Yuan[a,b,1], Zhenjie Liu[a,1], Jianping Zhao[c], Qin-Qin Wang[a], Aiyuan Zuo[a], Liting Huang[a], Hongwei Gao[a,*], Qiongming Xu[a,d,*], Ikhlas A. Khan[c,d], Shilin Yang[a]

[a] College of Pharmacy, Guangxi University of Chinese Medicine, Nanning 530000, China
[b] State Key Laboratory of Innovative Drug and Efficient Energy-Saving Pharmaceutical Equipment, Jiangxi University of Traditional Chinese Medicine, Nanchang 330004, China
[c] National Center for Natural Products Research, Research Institute of Pharmaceutical Sciences, School of Pharmacy, University of Mississippi, MS 38677, USA
[d] College of Pharmaceutical Science, Soochow University, Suzhou 215123, China

ARTICLE INFO

Keywords:
Coriander
Coriandrum Sativum L.
Compound 3
Anti-inflammation
NF-κB
MAPK

ABSTRACT

Coriander, *Coriandrum Sativum* L., is one of the commonest food and medicinal plants in many countries, but its chemical ingredients and pivotal role in anti-inflammatory activity have not been fully explored. The present study aimed to identify new compounds in the fruits of coriander and explore their anti-inflammatory activity. The compounds were isolated by chromatographic seperations and identified using spectroscopic and spectrometric methods. RAW264.7 macrophage cells were used to detect the anti-inflammatory activity of the compounds *via* Griess assay, western blotting, ELISA, and flow cytometry methods. The study resulted in the discovery of four new compounds, which were identified as: 4α-(furo[2,3-d]pyrimidin-6′-ylmethyl)-9α-propylnonolactone (**1**), 4-(formyloxy)-4-(6′-methylcyclohex-1-en-1-yl)butanoate(**2**), (7α,8α)-3α-hydroxyl-12,13α-dimethyl-5(6)-en-bicyclo[5,3,0]caprolactone (**3**), 7-methoxy-4-methyl-5,6-dihydro-7*H*-(2-hydroxypropan-2-yl)furo[2,3-f] coumarin (**4**). Compound **3** showed the highest anti-inflammatory activity with IC_{50} of 6.25 μM for an inhibitory effect on nitrite oxide (NO) level. In addition, compound **3** decreased the lipopolysaccharides-stimulated generations of ROS and the inflammatory cytokines (IL-6 and TNF-α). Mechanism exploration indicated that compound **3** suppressed inflammatory mediators' expression, like iNOS and COX-2. Furthermore, the NF-κB and MAPK pathways were involved in the anti-inflammatory process of compound **3**.

1. Introduction

Inflammation plays a crucial role in the progression of many diseases, excessive inflammation augments the activation of immune cells, which can destroy the tissues and body heath (Cárdeno et al., 2014; Franceschi & Campisi, 2014; Lee et al., 2020). Multiple pro-inflammatory mediators are over-produced when inflammation occurs and leads to a series of diseases, such as rheumatism, diabetes, and cardiovascular ailments (Golia et al., 2014; Karam, Chavez-Moreno, Koh, Akar, & Akar, 2017).

Macrophages cells have a critical role in the initiation of pro-inflammatory mediators. In LPS-stimulated macrophage cells, toll-like receptor 4 (TLR4) is activated, which can recruit MyD88, and subsequently cause the translocation of nuclear factor- κB (NF-κB) from the cytoplasm into the nucleus (Daddaoua et al., 2013). The activated NF-κB initiates the inflammatory regulators, such as interleukin-6 (IL-6), tumor necrosis factor-α (TNF-α), inducible nitric oxide synthase (iNOS), and cyclooxygenase-2 (COX-2) (Campestrini et al., 2020; Hoskin, Xiong, Esposito, & Lila, 2019; Katarzyna Popko, 2010; E.-A. Kim et al., 2019). The mitogen-activated protein kinase (MAPK) pathways play a significant role in the progression of inflammatory (Lee et al., 2020). In LPS-stimulated macrophage cells, TLR4 will form a dimer, which can activate the MAPK pathway, including JNK1/2, ERK1/2, and p38 MAPK (Han et al., 2020). The activated MAPKs mediates activation of COX-2 and iNOS in LPS-stimulated macrophage cells and promotes the inflammatory responses (Kim et al., 2011).

Abbreviations: LPS, lipopolysaccharides; TNF-α, tumor necrosis factor-α; NO, nitric oxide; COX-2, cyclooxygenase-2; iNOS, inducible nitric oxide synthase; NF-κB, nuclear factor-κB; IL-1β, interleukin-1β; IL-6, interleukin-6; MAPK, mitogen-activated protein kinase; JNK, c-Jun N-terminal kinase; ERK, extracellular regulated protein kinases; ROS, reactive oxygen species; $DCFH_2$-DA, 2′,7′-Dichlorodihydrofluorescein diacetate

* Corresponding authors at: College of Pharmacy, Guangxi University of Chinese Medicine, Nanning 530000, China (H. Gao).
E-mail addresses: gaohongwei06@126.com (H. Gao), xuqiongming@suda.edu.cn (Q. Xu).

[1] Renyikun Yuan and Zhenjie Liu equally contributed to this work.

https://doi.org/10.1016/j.jff.2020.104145
Received 13 June 2020; Received in revised form 18 July 2020; Accepted 27 July 2020
Available online 01 August 2020

Accumulated studies have confirmed that reactive oxygen species (ROS) are involved in the response of inflammation (Chelombitko, 2018). The enhanced generation of ROS will exacerbate inflammation and lead to tissue injury (Mittal, Siddiqui, Tran, Reddy, & Malik, 2014). Therefore, restraining the NF-κB signaling pathway, MAPK pathways, and ROS generation might be a potential strategy to attenuate inflammatory diseases.

Coriandrum Sativum L. (coriander) is an annual or biennial plant affiliated with the *Coriandrum* genus of *Umbelliferae* family (Laribi, Kouki, M'Hamdi, & Bettaieb, 2015; Lee et al., 2020). It is one of the oldest aromatic vegetables used as food or/and medicine for over 2000 years. The fresh green leaves called cilantro are commonly used as a vegetable, and the dried fruits are traditionally used as spice in cooking (Abascal & Yarnell, 2012). Coriander has been cultivated largely in North Africa, central Europe, and Asia. The green leaf is a rich source of vitamins, minerals, iron, but is low in cholesterol (Slavin & Lloyd, 2012). The dried ripe fruit of coriander is not only used as food and spice, it is also used as traditional medicine for the treatment of different ailments in many countries. Coriander alone or in combination with other traditional herbs has been used for treating many diseases like rheumatism, diabetes, cough, bronchitis, insomnia, gastrointestinal, and flatulence (Emamghoreishi, Khasaki, & Aazam, 2005; Gray & Flatt, 1999; Hosseinzadeh, Alaw Qotbi, Seidavi, Norris, & Brown, 2014). However, coriander's anti-inflammatory activity and underlying mechanisms are not clear.

In this study, LPS-stimulated RAW264.7 macrophage cells were used to unravel the anti-inflammatory activity of the ingredients in coriander fruits, four new compounds (**1**–**4**) were isolated and identified, along with four known ones. Compound **3** exhibited the highest anti-inflammatory activity for the inhibitory effect on NO level in Griess assay. The mechanism of anti-inflammatory activity for compound **3** was further investigated by using various cellular assays targeting IL-6, TNF-α, iNOS, COX-2, ROS, NF-κB, and MAPK signaling pathways. The results showed that compound **3** exerted an anti-inflammatory effect *via* the NF-κB and MAPK pathways and has an inhibitory effect on oxidative stress.

2. Materials and methods

2.1. Instruments and reagents

The specific optical rotation values, IR spectra, NMR data, and HR-ESI-MS were determined by Perkin-Elmer model 241 polarimeter, a Perkin-Elmer 983 G spectrometer, Varian Inova 500 spectrometer, and a Micromass Q-TOF2 spectrometer, respectively, as reported in a previous study (Kang et al., 2019). Medium pressure liquid chromatography (MPLC) system with a column (450 × 25 mm i.d.) was purchased from Bencao Tiancheng (Suzhou, China). The compounds were analyzed by HPLC Waters ACQUITY Arc with an ODS column (Waters ACQUITY UPLC HSS T3).

LPS (Escherichia coli O111:B4) and 2′,7′-Dichlorodihydrofluorescein diacetate ($DCFH_2$-DA) were acquired from Sigma-Aldrich (St. Louis, MO, USA). Fetal bovine serum (FBS) and dulbecco's modified eagle medium (DMEM) were acquired from Gibco Laboratories/Life Technologies (Grand Island, NY, USA). TNF-α and IL-6 ELISA kits were purchased from Neonbioscience (Shenzhen, China). The following antibodies were obtained from Cell Signaling Technology (Beverly, MA, USA): iNOS (13120), COX-2 (4842), GAPDH (5174), MAPK Family Antibody Sampler Kit (#9926), and NF-κB Family Member Antibody Sampler Kit (#4766).

2.2. Plant materials

The *Coriandrum Sativum* L. plants were grown in Qionggacun, Qusum, Shannan, Tibet, China and were verified by Prof. Xiaoran Li. When matured, the plants were harvested and dried in a ventilated area, then the fruits were collected. A voucher specimen (No. YS2018-10–11) was stored in the herbarium of the college of pharmacy at Guangxi University of Chinese Medicine.

2.3. Isolation and purification

Using a Soxhlet extractor, the dried fruits of *Coriandrum sativum* L. (10 kg) were powered into 100 mesh and extracted by petroleum ether to yield 6 L volatile oil. The left dregs were further extracted by methanol to obtain a liquid extract after removing the methanol. By adding proper hot water, the extract was sequentially extracted with petroleum ether, dichloromethane, and ethyl acetate to get 700.0 g, 192.5 g, and 143.0 g extract, respectively. The dichloromethane (192.5 g) extract was further separated by ethyl acetate and petroleum ether (10%, 20%, 30%, 40%, 60%, 80%, 100%) to yield seven fractions: Fr.A1, Fr.A2, Fr.A3, Fr.A4, Fr.A5, Fr.A6, and Fr.A7. Fr.A3 (27.0 g) was separated on a glass column packed with silicon gel (200–300 mesh) to obtain five fractions: Fr.A3-1, Fr.A3-2, Fr.A3-3, Fr.A3-4, and Fr.A3-5. Fr.A3-1 (13.5 g) and Fr.A3-2 (10.2 g) were further separated by using MPLC with a ODS column. Then the Sephadex LH-20 gel column and semi-preparative HPLC with C18 column were employed for further purification to yield compounds **1** (2.1 mg), **3** (8.2 mg), **4** (10.1 mg), and **5** (8.3 mg). Using the aforementioned methods, compounds **2** (8.1 mg) and **6** (20.4 mg) were separated in Fr.A4 (20.0 g). Using a different ratio of dichloromethane and methanol (90:10, 80:20, 70:30, 60:40, 40:60, 20:80, 0:100) as the mobile phase, the ethyl acetate extract (143.0 g) was separated on a reduced-pressure column packed with silicon (200–300 mesh) to obtain 7 fractions: Fr.B1–Fr.B7. Fr.B1 and Fr.B2 were separated using glass columns packed with silicon gel (200–300 mesh) eluting with different ratio of dichloromethane and methane (95:5, 90:10, 85:15, 80:20, 30:70, 50:50, 0:100) to give 7 fractions: Fr.B1-1–Fr.B1-7 and Fr.B2-1–Fr.B2-7, respectively. From Fr.B1-3 and Fr.B2-6, compounds **7** (22.4 mg) and **8** (17.6 mg), respectively, were obtained by using Sephadex LH-20 gel column and semi-preparative HPLC from.

Compound **1.** Light yellow powder; [α] −30.5 (c = 0.13, MeOH); IR (KBr) ν_{max}: 3323, 2945, 1775, 1674, 1652, 1255, 875 cm^{-1}; As shown in Table 1, the data of ^1H NMR (CD_3OD, 500 MHz) and ^{13}C NMR (CD_3OD, 125 MHz) were collected; HR-ESI-MS (positive ion mode) *m/z*: 317.1860 ([M + H]+, calcd for $C_{18}H_{25}N_2O_3$; 317.1865).

Compound **2.** White powder; [α] −31.0 (c = 0.15, MeOH); IR (KBr) ν_{max}: 3315, 3010, 1740, 1285, 780 cm^{-1}; As shown in Table 1, the data of ^1H NMR (CD_3OD, 500 MHz) and ^{13}C NMR (CD_3OD, 125 MHz) were collected; HR-ESI-MS (negative ion mode) *m/z*: 239.1287 ([M−H]-, calcd for $C_{13}H_{19}O_4$; 239.1283).

Compound **3.** White powder, [α] −34.5 (c = 0.16, MeOH); IR (KBr) ν_{max}: 3455, 2945, 3325, 1765, 1245, 865 cm^{-1}; As shown in Table 1, the data of ^1H NMR (CD_3OD, 500 MHz) and ^{13}C NMR (CD_3OD, 125 MHz) were collected; HR-ESI-MS (positive ion mode) *m/z*: 193.1234 ([M−H_2O + H]$^+$, calcd for $C_{12}H_{17}O_2$; 193.1229).

Compound **4.** Light yellow powder, [α] 0 (c = 0.11, MeOH); IR (KBr) ν_{max}: 3760, 3320, 2941, 1760, 1645, 1420, 1045, 650 cm^{-1}; As shown in Table 1, the data of ^1H NMR (CD_3OD, 500 MHz) and ^{13}C NMR (CD_3OD, 125 MHz) were collected; HR-ESI-MS (positive ion mode) *m/z*: 291.1234 ([M + H]$^+$, calcd for $C_{16}H_{19}O_5$; 291.1232). The scheme of purification showed in Fig. 1.

2.4. Cell Culture

RAW264.7 cells were purchased from the Cell Bank of Type Culture Collection of the Chinese Academy of Sciences (Shanghai, China). The cells were cultured in DMEM medium with 10% FBS and antibiotics at 37 °C in a humidified environment with 5% CO_2.

Table 1
NMR Spectroscopic Data for Compounds 1–4 (in CD_3OD).

No	1		2		3		4	
	δ_C	δ_H	δ_C	δ_H	δ_C	δ_H	δ_C	δ_H
1			174.0				101.7	
2	174.6		32.9	2.41 m	170.3		155.9	
3	40.9	1.91 m, 1.73 m	33.4	1.80 m	66.6	4.40 m	108.6	
4	49.5	2.41 m	85.5	4.04 m	31.0	2.19 m, 1.49 m	163.3	
5	26.4	2.12 m, 1.78 m	170.9	9.72 s	133.3		97.4	6.50 s
6	24.6	1.93 m, 1.48 m	50.6	3.66 s	135.7	6.54 d (3.1, 0.8)	154.4	
7	20.7	1.76 m, 1.59 m			43.2	2.62 m	160.5	
8	35.6	1.59 m, 1.16 m			85.6	4.02 m	103.8	6.30 s (1.0)
9	73.6	3.36 m			33.8	1.76 m	140.6	
10	27.5	1.33 m, 1.16 m			27.3	1.73 m, 1.43 m	17.8	2.20 s (1.0)
11	22.2	1.22 m			25.8	2.10 m, 1.46 m	55.1	3.92 s
12	12.9	0.85 t (7.1)			22.2	1.40 m		
13	48.5	3.34 d (3.3)			13.0	0.94 m		
14								
15								
16								
1′			130.8					
2′	148.6	9.11 s	135.6	6.75 dd (3.5, 7.0)			67.8	3.77 dd (7.0, 5.5)
3′			24.6	2.23 m, 2.34 m			25.8	2.88 dd (5.5), 2.56 dd (17.5, 7.1)
4′	164.2		20.4	1.55 m, 1.95 m			78.1	
5′			24.8	1.19 m, 2.07 m			19.5	1.31 s
6′	160.1		42.7	2.56 m			24.2	1.40 s
7′	120.9	7.65 brs (5.6, 5.4)	20.7	1.76 d				
8′	120.3							
9′	152.5	8.68 s						

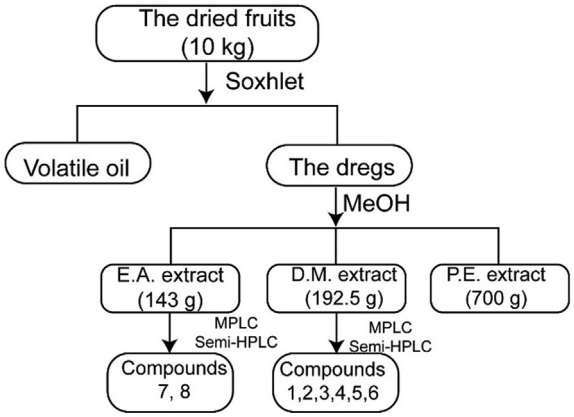

Fig. 1. Scheme of the purification process.

2.5. Cell viability assay

Cell viability studies were performed on the RAW264.7 cells at a density of 5×10^4 cell/ well (100 μL) in 96-well plates, which were subsequently treated with indicated compounds for 24 h. Cell viability was evaluated by MTT according to the manufacturer's protocols, the absorbance at 570 nm with a microplate reader (Molecular Devices, Sunnyvale, CA, USA) is recoded.

2.6. Griess reagent assay

RAW264.7 macrophages (2×10^5 cells/well) were seeded in 24-wells (500 μL) and pretreated with compounds at indicated concentrations for 1 h, and then treated with LPS for another 24 h. The collected medium was used to measure the nitrite levels by Griess reagent, the absorbance at 540 nm was detected by a microplate reader.

2.7. Flow cytometry assay

The cells were seeded in 24-well plates at a starting density of 2×10^5 cells per well (500 μL) and cultured in an incubator overnight. $DCFH_2$-DA was employed to analyze the ROS generation. At the end of compound **3** incubation for the indicated time point, $DCFH_2$-DA (1 μM, 30 min) was added to the medium, followed by signal collection by a FACScan Flow cytometer ((Becton-Dickinson, Franklin Lakes, NJ, USA).

2.8. Cytokines release assessment

Enzyme-linked immunosorbent assay (ELISA) was employed to detect the release of TNF-α and IL-6 according to the manufacture's protocols. Cells were seeded in 24-well plates at a starting density of 2×10^5 cells per well (500 μL) and pretreated with compound **3** for 1 h, then co-cultured with LPS for another16 h. The medium was collected to determine the release of the cytokines.

2.9. Western blotting analysis

RAW264.7 macrophages (1×10^6 cells/well) were seeded in dishes (3 mL), and which were subsequently pretreated with compound **3** for 1 h, then stimulated with LPS for another 4 h. Preparation of cell lysates, proteins' quantification, electrophoresis, and immunoblotting were performed as described previously (Kang et al., 2019; Yuan et al., 2019). The primary antibodies and secondary antibodies were diluted into 1:1000 and 1:10000, respectively. Chemiluminescence signals were determined by using a ChemiDoc™ MP Imaging System with Image Lab version 5.1 software (Bio-Rad, Hercules, CA, USA).

2.10. Immunofluorescence assay

Immunofluorescence assay was used to evaluate the translocation of NF-κB/p65. RAW264.7 cells were cultured in the confocal dish (SPL, Pocheon, Korea) overnight. At the end of the indicated time point for compound **3** incubation, the primary antibodies and fluorescence secondary antibodies were diluted into 1:100 and 1: 500, respectively. Cells were imaged using a Leica TCS SP8 laser confocal microscope (Leica, Germany) and the processing of images was performed by ImageJ software.

2.11. Data analysis

Two-sided Student's *t*-test was used to compare the differences between two groups. One-way-ANOVA and Dunńs multiple comparisons were used to compare the differences in more than two groups using GraphPad Prism 6.0 software. A *p*-value of < 0.05 was considered statistically significant.

3. Results and discussion

3.1. The chemical structure elucidation of compound 1–4

Compound **1** has a molecular formula of $C_{18}H_{24}N_2O_3$ in terms of its HR-ESI-MS $[M + H]^+$ data. In the ^1H NMR spectrum, a set of low field proton signals at δ_H 9.11 (1H, s, H-2′), 8.68 (1H, s, H-9′), 7.65 (1H, brs, H-7′) suggest the existence of a furo[2,3-d]pyrimidin group, which was supported by the series of low field carbon signals at δ_C 164.2 (C-4′), 160.1 (C-6′), 152.5 (C-9′), 148.6 (C-2′), 120.9 (C-7′) and 120.3 (C-8′), in its ^{13}C NMR spectrum. Combined with multiphase HSQC spectrum analysis, the proton signals of two methine groups at δ_H 3.36 (1H, m, H-9), 2.41 (1H, m, H-4), and those of seven methylene groups between δ_H 1.16–3.34 were observed in the high field part in its^1H NMR spectrum, as well as one methyl group at δ_H 0.85 (3H, t, J = 7.1 Hz, H-12). In its ^{13}C NMR spectrum, 18 carbon signals were observed. Among them, a methyl carbon, eight mesomethylene, five hypomethyl carbons, and six quaternary carbons were detected by the multiphase HSQC spectrum. The low field carbon signal at δ_C 174.6 (C-2) indicated the existence of a lactone group in the structure of compound 1. The downfield shiftings of C-9 at δ_C 73.6 (+37.0) and C-3 at δ_C 40.9 (+23.1) suggests the lactone group should be between C-3 and C-9, which was supported the HMBC correlations between H-3 at δ_H 1.91, 1.73, H-4 at δ_H 2.41, H-9 at δ_H 3.36 and C-2 at δ_C 174.6. Similarly, the downfield shift of C-4 at δ_C 49.5 (+13.1) indicated that the furo[2,3-d]pyrimidin group was linked to C-4 over a methylene group (C-13 at δ_C 48.5), which was also be supported by the HMBC correlations between H-4 at δ_H 2.41, H-13 at δ_H 3.34 and C-6′ at δ_C 160.1. The connections of the high field alkyl to both the furo[2,3-d]pyrimidin group and the lactone group to form the planar 4-(furo[2,3-d]pyrimidin-6′-ylmethyl)-9-propyl-nonolactone segment structure was determined by the analysis of the ^1H–^1H COSY spectrum. Moreover, the location of the propyl group at C-9 was confirmed by the evidence of HMBC correlations between H-11 at δ_H 1.22, H-10 at δ_H 1.33, 1.16, and C-9 at δ_C 73.6. The NOESY spectrum indicated the correlation between H-4 at δ_H 2.41 and H-9 at δ_H 3.36, suggesting that H-4 and H-9 has an identical configuration. Collectively, compound 1 was 4α-(furo[2,3-d]pyrimidin-6′-ylmethyl)-9α-propylnonolactone.

Compound 2 was calculated with a molecular formula of $C_{13}H_{20}O_4$ in terms of its HR-ESI-MS $[M-H]^-$ data. In the ^1H NMR spectrum, an olefinic proton signal at δ_H 6.75 (1H, dd, J = 7.0, 17.5 Hz, H-2′) suggests the existence of a carbon–carbon double bond, which was supported by the carbon signals at δ_C 130.8 (C-1′) and 135.6 (C-2′) in its ^{13}C NMR spectrum. The proton signals of one methyl at δ_H 1.76 (3H, d, J = 7.0 Hz, H-7′), five methylene at between δ_H 1.19–2.41, and one oxymethine at δ_H 4.04 (1H, m, H-4), as well as one methoxy at δ_H 3.66 (3H, s, H-6) were observed in its ^1H NMR and SHQC spectra. In the ^{13}C NMR spectrum, 13 carbon resonances were observed, which were attributed to two CH_3, five CH_2, four CH, and two quaternary carbons by the analysis of its HSQC spectrum. The HSQC correlation between H-5 at δ_H 9.72 and C-5 at δ_C 170.9 suggests that the existence of a formyl group. Accompanying with the HMBC correlations between H-6 at δ_H 3.66, H-2 at δ_H 2.41, H-3 at δ_H 1.80 and C-1 at δ_H 174.0, the molecular skeleton of compound **2** was established as butanoate by its H-H COSY spectrum. Similarly, the existence of a 6′-methylcyclohex-1-en-1 group was inferred.

Accompanying with the methine at C-4 instead of methyl, the downfield shifts of C-4 at δ_C 85.5 (+71.8) and C-3 at δ_C 33.4 (+18.3) suggests that both the 6′-methylcyclohex-1-en-1 group and the formyl group were linked to C-4 of the butanoate, which was supported by the HMBC correlations between H-4 at δ_H 4.04 and C-1′ at δ_C 130.8, C-2′ at δ_C 135.6, C-5 at δ_C 170.9. Collectively, compound **2** was 4-(formyloxy)-4-(6′-methylcyclohex-1-en-1-yl) butanoate named as coriander E.

Compound 3 was calculated with a molecular formula of $C_{12}H_{18}O_3$ in terms of the HR-ESI-MS $[M-H_2O + H]^+$ data. In the ^1H NMR spectrum, the signals of an olefinic proton at δ_H 6.54 (1H, d, J = 3.1 Hz, 0.8 Hz, H-6), two sets of methyl protons at δ_H 1.40 (3H, s, H-12), 0.94 (3H, d, J = 5.5 Hz, H-13), and two sets of oxymethine protons at δ_H 4.40 (1H, m, H-3), 4.02 (1H, m, H-8) were observed. In the ^{13}C NMR spectrum, 12 carbon resonances were observed including a signal for carbonyl carbon at δ_C 170.3 (C-2). Besides, two methyl carbons, three methylene carbons, five methine carbons, and two quaternary carbons were assigned by the analysis of its HSQC and ^1H NMR spectra. The downfield shifting of C-8 at δ_C 85.6 (+42.4) suggests the presence of a lactone group, which was supported the HMBC correlation between H-8 at δ_H 4.02 and C-2 at δ_C 170.3. The two olefinic carbon signals at δ_C 133.3, 135.7 indicated the existence of a carbon–carbon double bond in the structure of compound **3**, which should be attributed to C-5 and C-6 by the HMBC correlations between H-8 at δ_H 4.02, H-4 at δ_H 2.19 and C-6 at δ_C 135.7, and between H-3 at δ_H 4.40, H-7 at δ_H 2.62 and C-5 at δ_C 133.3. Accordingly, the basic skeleton of compound **3** was deduced to be a bicyclo[5, 3, 0]caprolactone by the analysis of its H-H COSY spectrum. In the HMBC spectra, Me-13 at δ_H 0.94 showed correlations to C-10 at δ_C 27.3 and C-8 at δ_C 85.6, and Me-12 at δ_H 1.40 showed correlations to C-4 at δ_C 31.0 and C-6 at δ_C 135.7, which indicated that the two methyl groups were located at C-9 and C-5 respectively. The NOESY spectrum indicated that there is a correlation between H-7 at δ_H 2.62 and H-9 at δ_H 1.76, H-3 at δ_H 4.40 and H-11 at δ_H 2.10, suggesting that H-7 and H-9 have the same spatial orientation, while H-7 and H-3 have an opposite orientation. Finally, compound **3** was (7α,8α)-3α-hydroxyl-12,13α-dimethyl-5(6)-en-bicyclo[5,3,0]caprolactone named coriander lactone C.

Compound 4 was calculated with a molecular formula of $C_{16}H_{18}O_5$ according to HR-ESI-MS $[M + H]^+$ data. In the ^1H NMR spectrum, a set of low field proton signals at δ_H 6.50 (1H, s, H-5), 6.30 (1H, s, H-8), suggests the existence of a benzene ring and lactone ring group, which was supported by the series of low field carbon signals at δ_C 101.7 (C-1), 155.9 (C-2), 108.6 (C-3), 163.3 (C-4), 97.4 (C-5),154.4 (C-6), 160.5 (C-7), 103.8 (C-8) and 140.6 (C-9), in its ^{13}C NMR spectrum. From the multiphase HSQC spectrum, a methine signal at δ_H 3.77 (1H, dd, J = 7.0, 5.6 Hz, H-2′), a methylene signal at δ_H 2.88 (1H, dd, J = 17.5, 5.6 Hz, H-3′), 2.56 (1H, dd, J = 7.1, 17.5 Hz, H-3′), and three methyl signals at δ_H 2.20 (3H, s, H-10), 1.31 (3H, s, H-5′), 1.40 (3H, s, H-6′), as well a methoxyl signal at δ_H 3.92 (3H, s, H-11) were respectively observed, corresponding to four methyl carbon, one mesomethylene, three hypomethyl carbons, and eight quaternary. The carbonyl carbon signal at δ_C 160.5 (C-7) indicated the existence of a lactone group in the structure of compound **4**. The carbon signals for three methyl at δ_C 19.5 (C-5′), 24.2 (C-6′) and 17.8 (C-10), and for a methoxy group at δ_C 55.1 (C-11) were observed in the HSQC spectrum. The downfield shifts of C-4 at δ_C 163.3 (+35.3) and C-6 at δ_C 154.4 (+26.4) suggests the methoxy group was linked to C-4, and the lactone group should be between C-6 and C-8, which was supported the HMBC correlations between H-5 at δ_H 6.50, H-10 at δ_H 2.20 and C-6 at δ_C 154.4. Combined with the HSQC and HMQC spectra, it was indicated that a coumarin skeleton was linked to the 9-methyl and the 4-methoxy group. The HMBC spectrum showed that C-4′ at δ_C of 78.1 was correlated to H-5′ at δ_H 1.31, H-6′ at δ_H 1.40, and H-3′ at δ_H 2.88, suggesting that a 4′-dimethyl-4′-propyl alcohol group was fused with C-2 and C-3 at the skeleton of 4-methoxy, 9-methyl coumarin to form the planar structure of compound **4**. Compound **4** was 7-methoxy-4-methyl-5,6-dihydro-7*H*-(2-hydroxypropan-2-yl)furo[2,3-f] coumarin, and named coriander D. The chemical structures of all compounds are displayed in Fig. 2. The HMBC, NOSEY, and COSY of Compound 1–4 are displayed in Fig. 3.

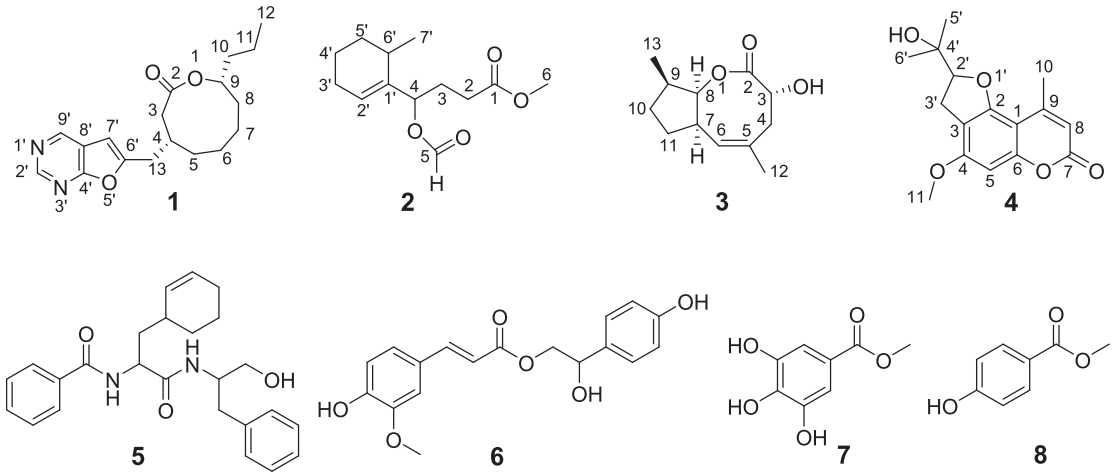

Fig. 2. The chemical structure of Compounds 1–8.

3.2. Effect of isolates on the nitrite level in RAW264.7 cells

The dried ripe fruit of coriander is recorded as a traditional medicine against various symptoms. However, the pharmacological research about the coriander's anti-inflammatory activity and the underlying mechanisms are not clear. Therefore, the suppressive effects of inflammation of coriander's bioactive products and their anti-inflammatory mechanisms using macrophages have been investigated for the first time in this study. NO, IL-6 and TNF-α are the mediators of the inflammatory response by inhibiting or promoting inflammation through numerous pathways. In this study, apart from four new compounds, four known compounds (**5–8**) were identified as aurantiamide, 2-O-E-feruloyl-1-(4-hydroxyphenyl) ethane-1, 2-diol, methyl gallate, and methyl p-hydroxybenzoate, respectively. The anti-inflammatory activity of all isolated compounds was investigated in terms of nitrite level in RAW264.7 cells. Nitrite is the mediator of an inflammatory response by inhibiting or promoting inflammation through numerous pathways. Connelly, et al. found that nitrite can activate NF-κB, and the activated NF-κB promotes the release of proinflammatory cytokines, including TNF-α and IL-6 to accelerate the progress of inflammation (Brasier, 2010). Therefore, inhibition of nitrite may suppress the inflammatory response. In this study, the anti-inflammatory effects of four new compounds (**1–4**) and four known ones (**5–8**) were investigated in terms of nitrite level in LPS-stimulated RAW264.7 macrophage cells using the Griess assay. Several compounds had anti-inflammatory activity, pretreatment with compounds suppressed LPS treatment stimulated production of nitrite on RAW264.7 macrophage cells, while compound **3** had a better inhibitory effect on nitrite level with IC_{50} of 6.25 μM than the other seven compounds, and treatment of compound **3** showed a dose-dependent decrease in the production of nitrite level (Fig. 4**A**). The cytotoxicity of 8 compounds was evaluated by MTT assay, and the results showed that all compounds almost have no cytotoxicity (data were not shown).

3.3. Suppression of inflammatory responses by compound *3*

The pro-inflammatory mediators like NO, iNOS, COX-2, *etc.*play a pivotal role in many inflammatory models due to their changes (Katarzyna Popko, 2010; Murakami & Ohigashi, 2007; Qingjie Xue, 2018). It has been demonstrated that excess NO production, most of which promotes the iNOS expression, subsequently regulates COX-2 expression in inflammatory models. Therefore, iNOS and COX-2 are potential targets for the prevention of inflammation (Murakami & Ohigashi, 2007). ROS is central to the progress of inflammatory, of which contributes to LPS-induced production of proinflammatory cytokines IL-6, TNF-α, and IL-1L, and the activation of the MAPK pathway (Gabriele, Pucci, Árvay, & Longo, 2018; Naik & Dixit, 2011; Patruno et al., 2015). The main factors of TNF-α and IL-6 are responsible for the induction of inflammatory response and also act as the markers of inflammation in LPS-induced macrophage cells. In the present study, pretreatment with compound **3** decreased iNOS and COX-2 proteins' expression in a dose-dependent manner in LPS-induced RAW264.7 cells (Fig. 4**B**). ROS is an important inflammatory response signal (Chelombitko, 2018). As shown in Fig. 4**C and D**, flow cytometry results indicated that treatment of LPS significantly increased ROS production in RAW264.7 cells, and compound **3** suppressed the generation of ROS in a dose-dependent manner. In addition to nitrite and ROS levels stimulated by LPS, the generation of TNF-α and IL-6, etc. will be also increased in RAW264.7 cells (Hochdörfer et al., 2013; Mittal et al., 2014). The results of this study indicates that compound **3** significantly decreased TNF-α and IL-6 level in LPS-stimulated RAW264.7 cells (Fig. 4**E and F**). Collectively, these data indicate that compound **3** exhibited both anti-inflammatory and anti-oxidant properties through suppressing the expression of iNOS and COX-2, the generation of ROS, and the releasing of TNF-α and IL-6 in LPS-stimulated RAW264.7 macrophage cells.

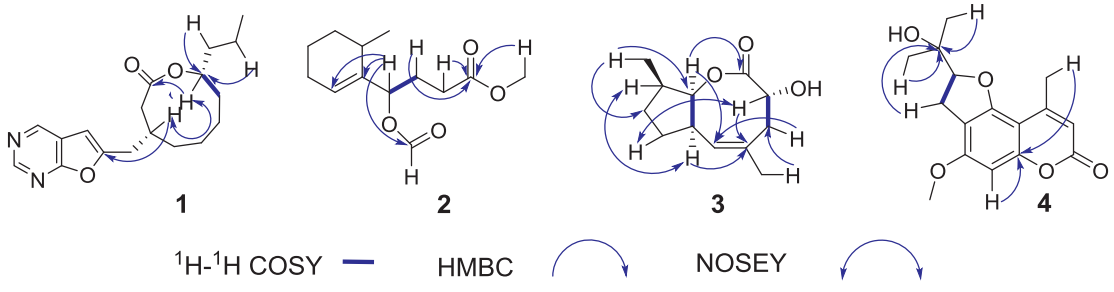

Fig. 3. The HMBC, NOSEY, and COSY of Compound 1–4.

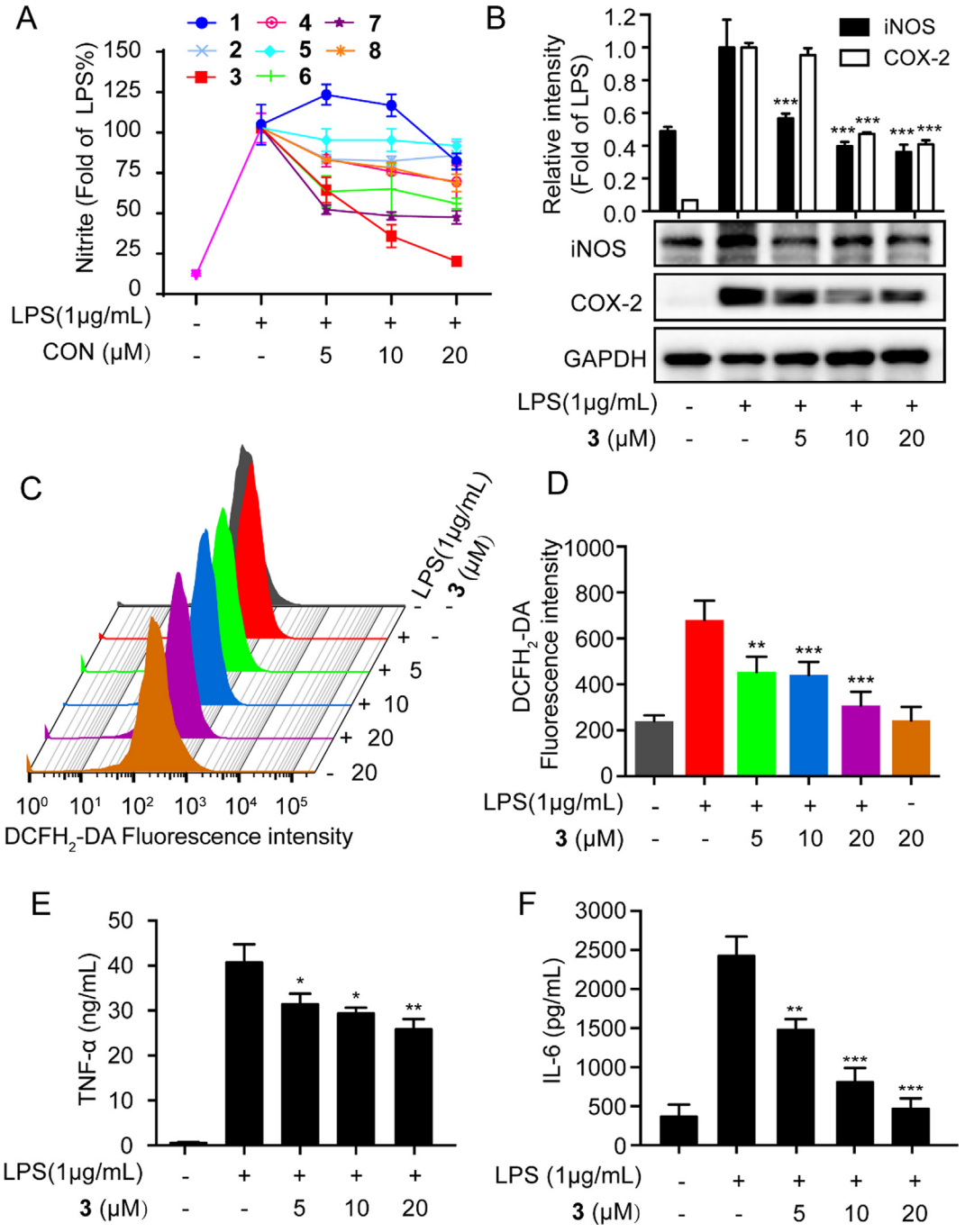

Fig. 4. Compound **3** decreased LPS-induced pro-inflammatory responses in RAW264.7 cells. (A) RAW264.7 cells were pretreated with the indicated concentration of the 8 compounds for 1 h, which were co-cultured with LPS (1 μg/mL) for another 24 h. The medium was collected to detect the nitrite level using the Griess assay. (B) RAW264.7 cells pretreated with compound **3** (5, 10, 20 μM) for 1 h, then co-cultured with LPS (1 μg/mL) for another 16 h. The proteins' expression of iNOS and COX-2 were determined by Western blotting assay. (C) RAW264.7 cells were pretreated with compound **3** (5, 10, 20 μM) for 1 h, then co-cultured with LPS (1 μg/mL) for another 6 h. Cells labeled with $DCFH_2$-DA (1 μM) for 30 min and determined by flow cytometry. (D) The statistical analysis of ROS fluorescence intensity. (E and F) RAW264.7 cells pretreated with compound **3** (5, 10, 20 μM) for 1 h, and co-cultured with LPS for another 24 h. The supernatants were collected and the pro-inflammatory cytokines TNF-α and IL-6 were determined by using the ELISA kit. $^{*}P < 0.05$, $^{**}P < 0.01$, $^{***}P < 0.001$ compared to the LPS alone group.

*3.4. Exploration of the role of compound **3** in the NF-κB and MAPKs pathways*

The transcriptional factor NF-κB is a member of Rel family and involves in the LPS-stimulated inflammatory progress (Lu et al., 2007), which has been validated as a regulator, and participates in the regulation of inflammatory factors, including iNOS, COX-2, IL-6, IL-1β, and TNF-α (Lawrence, 2009; Shang & Wu, 2020). The NF-κB signaling pathway also has a vital role in the chronic inflammatory disease. It has been found that NF-κB is inactive in the cytoplasm, IKKα and IKKβ are essential proteins in the activation of NF-κB, which promote the phosphorylation of IκB and subsequent degradation in LPS-induced RAW 264.7 cells (Castejon et al., 2019). NF-κB/p65 may be phosphorylated by the degraded IκB and translocated into the nucleus, which can further promote the release of proinflammatory cytokines and accelerate the inflammatory injury (Tak & Firestein, 2001). Therefore, we hypothesized that the NF-κB pathway may be involved in the anti-inflammatory activity of compound **3**. In this study, the expression of p-

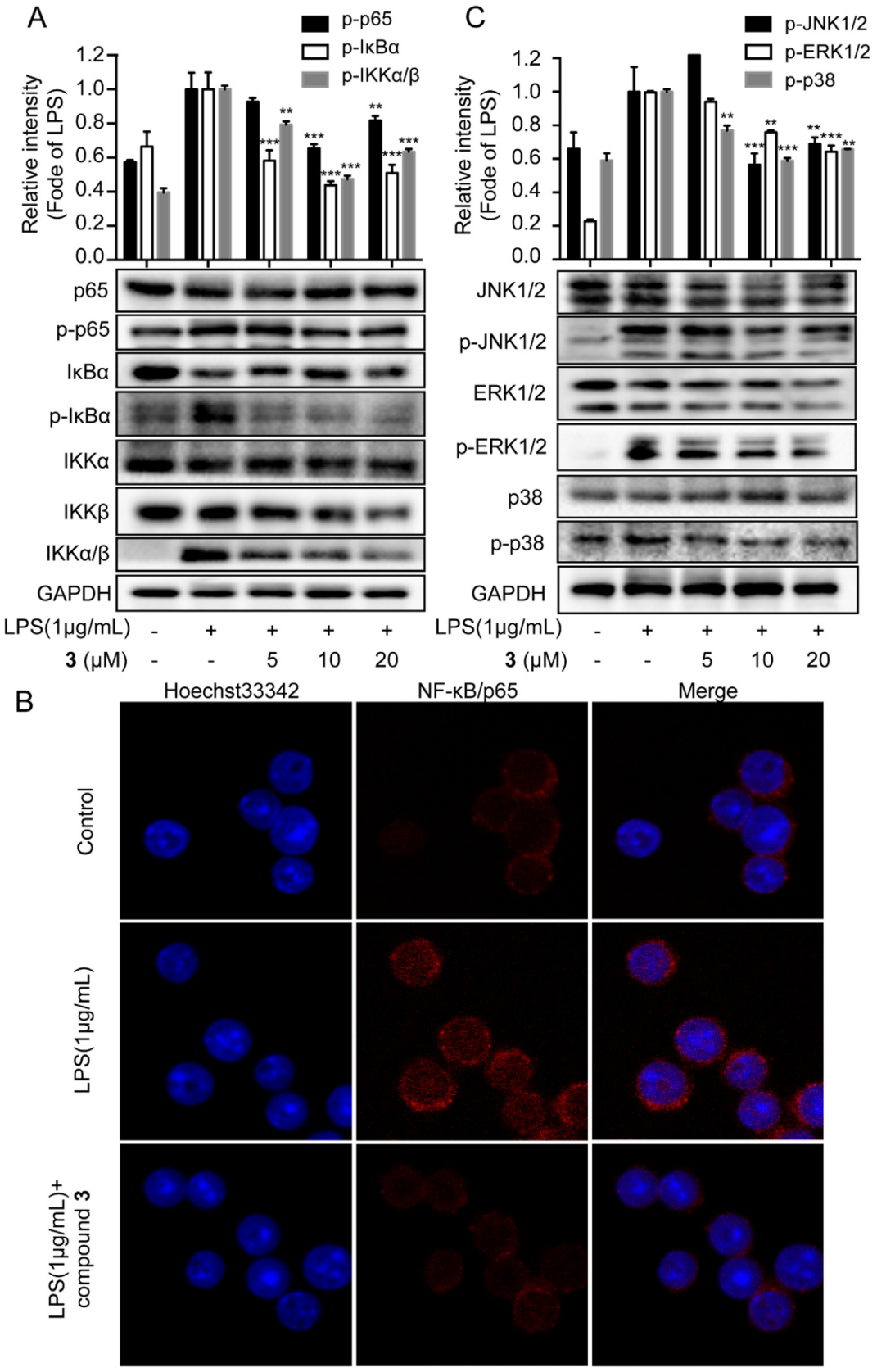

Fig. 5. NF-κB and MAPKs pathways were involved in compound **3**'s anti-inflammatory process. (A and C) RAW264.7 cells were pretreated with compound **3** (5, 10, 20 μM) for 1 h, and stimulated with LPS for another 4 h. The proteins' expression of p-p65, p65, p-IκB-α, IκB-α, p-IKK-α/β, IKK-α, IKK-β, p-JNK1/2, JNK1/2, p-ERK1/2, ERK1/2, p-p38, and p38 were determined by western blotting assay. (B) RAW264.7 cells were pretreated with compound **3** for 1 h, then co-treated with LPS for another 2 h. The translocation of p65 was determined by using the immunofluorescence assay described in the Methods sections. The primary antibody anti-NF-κB/p65 (1:100) and secondary antibody goat anti-Rabbit Alexa Fluor 568 (1:200). $^{*}P < 0.05$, $^{**}P < 0.01$, and $^{***}P < 0.001$, compared to LPS alone group.

p65, p-IKKα/β, p-IκBα increased, which were markedly suppressed by compound **3** in LPS-induced RAW264.7 cells (Fig. 5**A**). Furthermore, the immunofluorescence staining analysis indicates that compound **3** suppressed the translocation of NF-κB/p65 into the nucleus (Fig. 5**B**). These results suggest that the NF-κB pathway was involved in the anti-inflammatory activity of compound **3**.

The MAPK signaling pathway, including JNK1/2, ERK1/2, and p38MAPK, are involved in cellular signaling cascades wherein intracellular or extracellular stimuli induce inflammation, and has a response to inflammation (Chen et al., 2015). Previous studies validated that the MAPK pathway has a mediated effect on the activation of iNOS and COX-2 in LPS-induced macrophage cells (Zhang, Luna-Vital, & Gonzalez de Mejia, 2019). Therefore, the effects of compound **3** on the activation of JNK1/2, ERK1/2, and p38MAPK in LPS-induced RAW264.7 cells were evaluated by western blotting assay. As shown in Fig. 2B, pretreatment with compound **3** sharply decreased p-JNK1/2, p-ERK1/2, and p-p38MAPK expression in RAW264.7 cells induced by LPS, but did not affect total JNK1/2, ERK1/2, and p38MAPK expression (Fig. 5**C**). Those results demonstrated that compound **3** could prevent extracellular stimuli in LPS-stimulated macrophage cells, by inhibiting the phosphorylation of MAPKs. The findings indicate that NF-κB and MAPK pathways might account for compound **3**′s anti-inflammatory activity.

4. Conclusions

In this study, we investigated the bioactive products of coriander and their anti-inflammatory mechanisms in chemical and pharmacological perspective, results demonstrated that eight compounds were identified from the dried ripe fruit of coriander, including four new compounds (**1**–**4**) and four known compounds (**5**–**8**), and compound **3** showed the most significant anti-inflammatory effect through inhibiting nitrite level, ROS production, and the generation of IL-6 and TNF-α. The mechanism exploration indicates that NF-κB and MAPKs pathways participated in compound **3**′s anti-inflammatory effect. Collectively, our findings indicate that compound **3** exhibits a prominent inhibitory effect on inflammation.

5. Author information

H. Gao and Q. Xu designed the research. H. Gao, Z. Liu and J. Zhao conducted chemical experiments. R. Yuan, Q. Wang, A. Zuo, L. Huang, and H. Gao conducted anti-inflammatory experiments *in vitro*. R. Yuan, Z. Liu, H. Gao, and Q. Xu wrote the manuscript. I. A. Khan and S. Yang revised the manuscript. All authors reviewed the manuscript.

Ethics Statements

Our research "**Novel Compounds in Fruits of Coriander (*Coriandrum Sativum* L.) with Anti-inflammatory Activity**" did not include any human subjects and animal experiments.

Declaration of Competing Interest

None.

Acknowledgments

We would like to appreciate the support from the National Natural Science Foundation of China (NSFC, 81803807, 81860711), Guangxi Natural Science Foundation (2018JJB140265, China), Ph.D. Fund of Guangxi University of Chinese Medicine (B170023), Guangxi Science and Technology Base and Talent Special Project (2018AD19034, China), the project of Guangxi overseas "100 persons plan" high-level expert, College Students' Innovative Entrepreneurial Training Plan Program in Guangxi University of Chinese Medicine, and the Project of cultivating High-level Talent Teams in the Qi Huang Project of Guangxi University of Chinese Medicine (2018002).

Appendix A. Supplementary material

Supplementary data to this article can be found online at https://doi.org/10.1016/j.jff.2020.104145.

References

Abascal, K., & Yarnell, E. (2012). Cilantro—Culinary Herb or Miracle Medicinal Plant? *Alternative and Complementary Therapies, 18*(5), 259–264. https://doi.org/10.1089/act.2012.18507.

Brasier, A. R. (2010). The nuclear factor-kappaB-interleukin-6 signalling pathway mediating vascular inflammation. *Cardiovascular Research, 86*(2), 211–218. https://doi.org/10.1093/cvr/cvq076.

Campestrini, L. H., Rasera, G. B., de Camargo, A. C., Franchin, M., Nani, B. D., Rosalen, P. L., ... Alencar, S. M. (2020). Alkaline conditions better extract anti-inflammatory polysaccharides from winemaking by-products. *Food Research International, 131*, Article 108532. https://doi.org/10.1016/j.foodres.2019.108532.

Cárdeno, A., Magnusson, M. K., Strid, H., Alarcón de La Lastra, C., Sánchez-Hidalgo, M., & Öhman, L. (2014). The unsaponifiable fraction of extra virgin olive oil promotes apoptosis and attenuates activation and homing properties of T cells from patients with inflammatory bowel disease. *Food Chemistry, 161*, 353–360. https://doi.org/10.1016/j.foodchem.2014.04.016.

Castejon, M. L., Sánchez-Hidalgo, M., Aparicio-Soto, M., González-Benjumea, A., Fernández-Bolaños, J. G., & Alarcón-de-la-Lastra, C. (2019). Olive secoiridoid oleuropein and its semisynthetic acetyl-derivatives reduce LPS-induced inflammatory response in murine peritoneal macrophages via JAK-STAT and MAPKs signaling pathways. *Journal of Functional Foods, 58*, 95–104. https://doi.org/10.1016/j.jff.2019.04.033.

Chelombitko, M. A. (2018). Role of Reactive Oxygen Species in Inflammation: A Minireview. *Moscow University Biological Sciences Bulletin, 73*(4), 199–202. https://doi.org/10.3103/S009639251804003X.

Chen, W. C., Yen, C. S., Huang, W. J., Hsu, Y. F., Ou, G., & Hsu, M. J. (2015). WMJ-S-001, a novel aliphatic hydroxamate derivative, exhibits anti-inflammatory properties via MKP-1 in LPS-stimulated RAW264.7 macrophages. *British Journal of Pharmacology, 172*(7), 1894–1908. https://doi.org/10.1111/bph.13040.

Daddaoua, A., Martínez-Plata, E., Ortega-González, M., Ocón, B., Aranda, C. J., Zarzuelo, A., ... Martínez-Augustin, O. (2013). The nutritional supplement Active Hexose Correlated Compound (AHCC) has direct immunomodulatory actions on intestinal epithelial cells and macrophages involving TLR/MyD88 and NF-κB/MAPK activation. *Food Chemistry, 136*(3), 1288–1295. https://doi.org/10.1016/j.foodchem.2012.09.039.

Emamghoreishi, M., Khasaki, M., & Aazam, M. F. (2005). Coriandrum sativum: Evaluation of its anxiolytic effect in the elevated plus-maze. *Journal of Ethnopharmacology, 96*(3), 365–370. https://doi.org/10.1016/j.jep.2004.06.022.

Franceschi, C., & Campisi, J. (2014). Chronic Inflammation (Inflammaging) and Its Potential Contribution to Age-Associated Diseases. *The Journals of Gerontology: Series A, 69*(Suppl_1), S4–S9. https://doi.org/10.1093/gerona/glu057.

Gabriele, M., Pucci, L., Árvay, J., & Longo, V. (2018). Anti-inflammatory and antioxidant effect of fermented whole wheat on TNFα-stimulated HT-29 and NF-κB signaling pathway activation. *Journal of Functional Foods, 45*, 392–400. https://doi.org/10.1016/j.jff.2018.04.029.

Golia, E., Limongelli, G., Natale, F., Fimiani, F., Maddaloni, V., Pariggiano, I., ... Calabrò, P. (2014). Inflammation and Cardiovascular Disease: From Pathogenesis to Therapeutic Target. *Current Atherosclerosis Reports, 16*(9), 435. https://doi.org/10.1007/s11883-014-0435-z.

Gray, A. M., & Flatt, P. R. (1999). Insulin-releasing and insulin-like activity of the traditional anti-diabetic plant Coriandrum sativum (coriander). *British Journal of Nutrition, 81*(3), 203–209. https://doi.org/10.1017/S0007114599000392.

Han, Y., Zhang, X., Qi, R., Li, X., Gao, Y., Zou, Z., ... Qi, Y. (2020). Lucyoside B, a triterpenoid saponin from Luffa cylindrica, inhibits the production of inflammatory mediators via both nuclear factor-κB and activator protein-1 pathways in activated macrophages. *Journal of Functional Foods, 69*, Article 103941. https://doi.org/10.1016/j.jff.2020.103941.

Hochdörfer, T., Tiedje, C., Stumpo, D. J., Blackshear, P. J., Gaestel, M., & Huber, M. (2013). LPS-induced production of TNF-α and IL-6 in mast cells is dependent on p38 but independent of TTP. *Cell Signal, 25*(6), 1339–1347. https://doi.org/10.1016/j.cellsig.2013.02.022.

Hoskin, R. T., Xiong, J., Esposito, D. A., & Lila, M. A. (2019). Blueberry polyphenol-protein food ingredients: The impact of spray drying on the in vitro antioxidant activity, anti-inflammatory markers, glucose metabolism and fibroblast migration. *Food Chemistry, 280*, 187–194. https://doi.org/10.1016/j.foodchem.2018.12.046.

Hosseinzadeh, H., Alaw Qotbi, A. A., Seidavi, A., Norris, D., & Brown, D. (2014). Effects of different levels of coriander (Coriandrum sativum) seed powder and extract on serum biochemical parameters, microbiota, and immunity in broiler chicks. *The Scientific World Journal, 2014*. https://doi.org/10.1155/2014/628979.

Kang, N., Yuan, R., Huang, L., Liu, Z., Huang, D., Huang, L., ... Yang, S. (2019). Atypical Nitrogen-Containing Flavonoid in the Fruits of Cumin (Cuminum cyminum L.) with Anti-inflammatory Activity. *Journal of Agricultural and Food Chemistry, 67*(30), 8339–8347. https://doi.org/10.1021/acs.jafc.9b02879.

Karam, B. S., Chavez-Moreno, A., Koh, W., Akar, J. G., & Akar, F. G. (2017). Oxidative stress and inflammation as central mediators of atrial fibrillation in obesity and

diabetes. *Cardiovascular Diabetology, 16*(1), https://doi.org/10.1186/s12933-017-0604-9.

Katarzyna Popko (2010). Proinflammatory cytokines Il-6 and TNF-α and the development of inflammation in obese subjects. doi:10.1186/2047-783x-15-s2-120.

Kim, A. R., Lee, M.-S., Shin, T.-S., Hua, H., Jang, B.-C., Choi, J.-S., ... Kim, H.-R. (2011). Phlorofucofuroeckol A inhibits the LPS-stimulated iNOS and COX-2 expressions in macrophages via inhibition of NF-κB, Akt, and p38 MAPK. *Toxicology in Vitro, 25*(8), 1789–1795. https://doi.org/10.1016/j.tiv.2011.09.012.

Kim, E.-A., Kim, S.-Y., Kim, J., Oh, J.-Y., Kim, H.-S., Yoon, W.-J., ... Heo, S.-J. (2019). Tuberatolide B isolated from Sargassum macrocarpum inhibited LPS-stimulated inflammatory response via MAPKs and NF-κB signaling pathway in RAW264.7 cells and zebrafish model. *Journal of Functional Foods, 52*, 109–115. https://doi.org/10.1016/j.jff.2018.10.030.

Laribi, B., Kouki, K., M'Hamdi, M., & Bettaieb, T. (2015). Coriander (Coriandrum sativum L.) and its bioactive constituents. *Fitoterapia, 103*, 9–26. https://doi.org/10.1016/j.fitote.2015.03.012.

Lawrence, T. (2009). The nuclear factor NF-kappaB pathway in inflammation. *Cold Spring Harbor Perspectives in Biology, 1*(6), https://doi.org/10.1101/cshperspect.a001651.

Lee, J.-W., Kim, Y.-S., Dong, X., Park, J.-S., Shin, W.-B., Kim, S.-J., ... Park, P.-J. (2020). Anti-inflammatory effect of Rhodiola crenulata extracts through the down-regulation of MyD88 dependent pathway and induction of autophagy. *Journal of Functional Foods, 64*, Article 103703. https://doi.org/10.1016/j.jff.2019.103703.

Lu, D. Y., Tang, C. H., Liou, H. C., Teng, C. M., Jeng, K. C., Kuo, S. C., ... Fu, W. M. (2007). YC-1 attenuates LPS-induced proinflammatory responses and activation of nuclear factor-kappaB in microglia. *British Journal of Pharmacology, 151*(3), 396–405. https://doi.org/10.1038/sj.bjp.0707187.

Mittal, M., Siddiqui, M. R., Tran, K., Reddy, S. P., & Malik, A. B. (2014). Reactive oxygen species in inflammation and tissue injury. *Antioxid Redox Signal, 20*(7), 1126–1167. https://doi.org/10.1089/ars.2012.5149.

Murakami, A., & Ohigashi, H. (2007). Targeting NOX, INOS and COX-2 in inflammatory cells: Chemoprevention using food phytochemicals. *International Journal of Cancer, 121*(11), 2357–2363. https://doi.org/10.1002/ijc.23161.

Naik, E., & Dixit, V. M. (2011). Mitochondrial reactive oxygen species drive proinflammatory cytokine production. *The Journal of Experimental Medicine, 208*(3), 417–420. https://doi.org/10.1084/jem.20110367.

Patruno, A., Fornasari, E., Di Stefano, A., Cerasa, L. S., Marinelli, L., Baldassarre, L., ... Cacciatore, I. (2015). Synthesis of a Novel Cyclic Prodrug of S-Allyl-glutathione Able To Attenuate LPS-Induced ROS Production through the Inhibition of MAPK Pathways in U937 Cells. *Molecular Pharmaceutics, 12*(1), 66–74. https://doi.org/10.1021/mp500431r.

Qingjie Xue (2018). Regulation of iNOS on Immune Cells and Its Role in Diseases. doi:10.3390/ijms19123805.

Shang, N., & Wu, J. (2020). Egg-derived Tripeptide IRW Attenuates LPS-induced Osteoclastogenesis in RAW 264.7 Macrophages via Inhibition of Inflammatory Responses and NF-κB/MAPK Activation. *Journal of Agricultural and Food Chemistry.*. https://doi.org/10.1021/acs.jafc.0c01159.

Slavin, J. L., & Lloyd, B. (2012). Health benefits of fruits and vegetables. *Advances in nutrition (Bethesda, Md.), 3*(4), 506–516. https://doi.org/10.3945/an.112.002154.

Tak, P. P., & Firestein, G. S. (2001). NF-κB: A key role in inflammatory diseases. *The Journal of Clinical Investigation, 107*(1), 7–11. https://doi.org/10.1172/JCI11830.

Yuan, R., Huang, L., Du, L.-J., Feng, J.-F., Li, J., Luo, Y.-Y., ... Feng, Y.-L. (2019). Dihydrotanshinone exhibits an anti-inflammatory effect in vitro and in vivo through blocking TLR4 dimerization. *Pharmacological Research, 142*, 102–114. https://doi.org/10.1016/j.phrs.2019.02.017.

Zhang, Q., Luna-Vital, D., & Gonzalez de Mejia, E. (2019). Anthocyanins from colored maize ameliorated the inflammatory paracrine interplay between macrophages and adipocytes through regulation of NF-κB and JNK-dependent MAPK pathways. *Journal of Functional Foods, 54*, 175–186. https://doi.org/10.1016/j.jff.2019.01.016.